



# Kent Academic Repository

Dixey, Richard J. C., Falsaperna, Mario, Bulled, Jonathan M., Orlandi, Fabio, Manuel, Pascal, Hester, James R., Mukherjee, Paromita, Dutton, Siân E. and Saines, Paul J. (2024) *Magnetic order in holmium and erbium formate: Parent frameworks for a potential random spin chain paramagnet*. *Journal of Solid State Chemistry*, 336 . ISSN 0022-4596.

## Downloaded from

<https://kar.kent.ac.uk/105929/> The University of Kent's Academic Repository KAR

## The version of record is available from

<https://doi.org/10.1016/j.jssc.2024.124770>

## This document version

Publisher pdf

## DOI for this version

## Licence for this version

CC BY (Attribution)

## Additional information

## Versions of research works

### Versions of Record

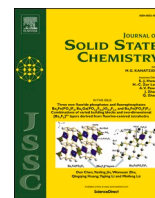
If this version is the version of record, it is the same as the published version available on the publisher's web site. Cite as the published version.

### Author Accepted Manuscripts

If this document is identified as the Author Accepted Manuscript it is the version after peer review but before type setting, copy editing or publisher branding. Cite as Surname, Initial. (Year) 'Title of article'. To be published in **Title of Journal** , Volume and issue numbers [peer-reviewed accepted version]. Available at: DOI or URL (Accessed: date).

### Enquiries

If you have questions about this document contact [ResearchSupport@kent.ac.uk](mailto:ResearchSupport@kent.ac.uk). Please include the URL of the record in KAR. If you believe that your, or a third party's rights have been compromised through this document please see our [Take Down policy](https://www.kent.ac.uk/guides/kar-the-kent-academic-repository#policies) (available from <https://www.kent.ac.uk/guides/kar-the-kent-academic-repository#policies>).



## Magnetic order in holmium and erbium formate: Parent frameworks for a potential random spin chain paramagnet

Richard J.C. Dixey<sup>a</sup>, Mario Falsaperla<sup>a</sup>, Jonathan M. Bulled<sup>b</sup>, Fabio Orlandi<sup>c</sup>, Pascal Manuel<sup>c</sup>, James R. Hester<sup>d</sup>, Paromita Mukherjee<sup>e</sup>, Siân E. Dutton<sup>e</sup>, Paul J. Saines<sup>a,\*</sup>

<sup>a</sup> School of Chemistry and Forensic Science, Ingram Building, University of Kent, Canterbury, CT2 7NH, United Kingdom

<sup>b</sup> Inorganic Chemistry Laboratory, South Parks Road, Oxford, OX1 3QR, United Kingdom

<sup>c</sup> ISIS Facility, STFC, Rutherford Appleton Laboratory, Chilton, Didcot, OX11 0QX, United Kingdom

<sup>d</sup> Australian Nuclear Science and Technology Organisation, Lucas Heights, NSW, 2234, Australia

<sup>e</sup> Cavendish Laboratory, University of Cambridge, JJ Thomson Avenue, Cambridge, CB3 0HE, United Kingdom

### ARTICLE INFO

#### Keywords:

Low dimensional  
Magnetism  
Metal-organic framework  
Neutron diffraction

### ABSTRACT

This work uses a combination of neutron diffraction and bulk property measurements to establish the low temperature magnetic states in the dense metal-organic frameworks  $\text{Ho}(\text{HCO}_2)_3$  and  $\text{Er}(\text{HCO}_2)_3$ ; whose structures feature chains of face-sharing  $\text{LnO}_9$  polyhedra packed into a triangular lattice. Below 0.7 K  $\text{Ho}(\text{HCO}_2)_3$  is found to adopt a state in which the magnetic moment on its ferromagnetic chains vary from neighbouring chains but the sum around each triangle is constant.  $\text{Er}(\text{HCO}_2)_3$  is found to be the first lanthanide formate to adopt an ordered magnetic state with antiferromagnetic coupling within its chains near 50 mK. The potential to combine the ferromagnetic and antiferromagnetic coupling within chains associated with Ho and Er cations, respectively, in the same compound has also been explored via the series  $\text{Ho}_{1-x}\text{Er}_x(\text{HCO}_2)_3$ .  $\text{Ho}_{0.5}\text{Er}_{0.5}(\text{HCO}_2)_3$  remains paramagnetic to 0.4 K, suggesting it may be a starting point to search for a random spin chain paramagnet.

### 1. Introduction

Low dimensional magnets have long provided an important playground for the discovery and exploitation of unconventional physics [1]. This includes the earliest studies of soliton excitations in  $\text{CsNiF}_3$  [2–4], magnetic frustration in spin-chains with combinations of ferromagnetic and antiferromagnetic coupling [5,6], the observation of the spin–Peierl’s transition in linear chains of  $\text{Cu}^{2+}$  in  $\text{CuGeO}_3$  [7–10], the likely presence of random spin chain paramagnetism in  $\text{Sr}_3\text{CuPt}_{1-x}\text{Ir}_x\text{O}_6$  [11–13] and contemporary research into quantum information transport in spin-chain compounds [14]. In such materials the strength of the magnetic coupling varies greatly along different dimensions of their crystal structures. Most well studied low dimensional magnets are, however, purely inorganic materials such as metal oxides. These typically adopt close packed structures in which it is difficult to isolate their low dimensional units. In this respect dense metal-organic frameworks (MOFs), in which cations are connected to form extended structures via organic ligands, are promising candidates for hosting 1D and 2D magnetic units [15–17]. It is possible to design MOFs with inorganic chains or sheets that host strong magnetic interactions within them, linked by

organic ligands that only provide much weaker magnetic coupling in other dimensions [15–18]. The magnetic response of a range of MOF families, including formates [19], oxalates [20] and succinates [21,22] can be interpreted in terms of low dimensional behaviour. The majority of knowledge of magnetic order in MOFs is, however, based on bulk property measurements such as magnetic susceptibility and heat capacity that do not provide direct understanding on the atomic scale equivalent to that accessible using neutron scattering [15].

Amongst low dimensional magnetic MOFs the  $\text{Ln}(\text{HCO}_2)_3$  phases, where Ln can vary between  $\text{Ce}^{3+}$  to  $\text{Er}^{3+}$  amongst the magnetic lanthanides, have attracted significant attention in recent years. In these materials, which adopt  $R3m$  symmetry, there are face-sharing chains of  $\text{LnO}_9$  polyhedra that are packed into a triangular lattice in which neighbouring chains are connected by the carboxylate-based formate linkers [23]. Recent interest in these magnets began with studies of Gd  $(\text{HCO}_2)_3$  as a magnetocaloric due to its very promising entropically driven magnetic cooling properties [23]. Furthermore it has been shown that the magnetocaloric properties of  $\text{Tb}(\text{HCO}_2)_3$  can be optimised for applications above 4 K under the relatively modest field changes of less than 2 T that can be produced using permanent magnets [24]. Analysis

\* Corresponding author.

E-mail address: [P.Saines@kent.ac.uk](mailto:P.Saines@kent.ac.uk) (P.J. Saines).

<https://doi.org/10.1016/j.jssc.2024.124770>

Received 1 February 2024; Received in revised form 3 May 2024; Accepted 8 May 2024

Available online 9 May 2024

0022-4596/© 2024 The Authors. Published by Elsevier Inc. This is an open access article under the CC BY license (<http://creativecommons.org/licenses/by/4.0/>).

of the diffuse magnetic scattering obtained from neutron diffraction measurements of  $\text{Tb}(\text{HCO}_2)_3$  suggested this arises from ferromagnetic chains of Ising spins coupled by weaker interchain antiferromagnetic interactions. This is in contrast with the antiferromagnetic coupling in  $\text{Gd}(\text{HCO}_2)_3$  and, thus, it appears that the optimised magnetocaloric properties arise from the ease with which ferromagnetic Ising chains can be aligned with the applied field once the antiferromagnetic coupling between them is suppressed [24,25]. Subsequent neutron scattering studies of  $\text{Tb}(\text{HCO}_2)_3$  identified the emergence of ferromagnetic order in the  $\text{TbO}_9$  chains at 1.6 K [26]. This order is supported by the antiferromagnetic interchain interactions, which due to frustration only lead to short range correlations in the other two dimensions. The interchain interactions appear to be about two orders of magnitude weaker than the intrachain ones [26]. This phase can be interpreted as a realisation of the triangular Ising antiferromagnet (TIA) if we treat the spins of each chain to be a single emergent moment. On cooling  $\text{Tb}(\text{HCO}_2)_3$  to 1.2 K there is a transition to a second magnetic state in which the magnetic moment of neighbouring chains is modulated by a second propagation vector [27]. The sum of the spins around each triangle in the 2D lattice is equal and it thus resembles the emergent charge ordered (ECO) state reported in Kagome lattices in which the sum of the magnetic spins around a triangle can be thought of as an emergent magnetic charge [28–30].

It has previously been reported that the paramagnetic phase of  $\text{Ho}(\text{HCO}_2)_3$  has similar, although weaker, correlations to  $\text{Tb}(\text{HCO}_2)_3$ , with ferromagnetic chains and frustrated antiferromagnetic correlations between the chains [27]. This is consistent with its magnetocaloric properties also being optimised for modest applied fields, albeit to a significantly weaker extent than  $\text{Tb}(\text{HCO}_2)_3$  [24]. In  $\text{Ho}(\text{HCO}_2)_3$  the correlated paramagnetic phase is retained down to 1.5 K and how it evolves towards magnetic order at lower temperatures has not previously been examined. There is no indication of significant magnetic diffuse scattering in the other  $\text{Ln}(\text{HCO}_2)_3$  phases down to 1.5 K [27]. In this study we examine the magnetic ordering of  $\text{Ho}(\text{HCO}_2)_3$  finding it undergoes a transition directly from the correlated paramagnetic phase to a state similar to the reported ECO phase of  $\text{Tb}(\text{HCO}_2)_3$ . We have also investigated the magnetic ordering in  $\text{Er}(\text{HCO}_2)_3$ , which appears to be the only other  $\text{Ln}(\text{HCO}_2)_3$  phase to exhibit magnetic order above 50 mK [31,32], finding that unlike the Tb and Ho analogues it has antiferromagnetic order within its chains. This inspired us to make a solid solution  $\text{Ho}_{1-x}\text{Er}_x(\text{HCO}_2)_3$  to examine the bulk properties of these compounds to explore the effect on the magnetic properties of combining ferromagnetic and antiferromagnetic intrachain coupling. It was found that  $\text{Ho}_{0.5}\text{Er}_{0.5}(\text{HCO}_2)_3$  exhibits paramagnetic behaviour down to 0.4 K, making it a possible starting point for a random spin chain paramagnet in which there are a random mixture of ferromagnetic and antiferromagnetic intrachain coupling.

## 2. Materials and methods

Following a literature procedure [27], samples of  $\text{Ho}_{1-x}\text{Er}_x(\text{HCO}_2)_3$  ( $x = 0, 0.1, 0.2, 0.3, 0.4, 0.5, 0.6, 0.7, 0.8, 0.9, 1.0$ ) were synthesised by dissolving 2 g of the metal precursors,  $\text{Ho}(\text{NO}_3)_3 \cdot 5\text{H}_2\text{O}$  and  $\text{Er}(\text{NO}_3)_3 \cdot 5\text{H}_2\text{O}$ , in the appropriate molar ratios, in 4.75 ml formic acid (98+%, Fisher Chemicals) with the addition of 0.25 ml ethanol. After several minutes of stirring at ambient temperature, the release of  $\text{NO}_y$  gases could be observed alongside the precipitation of pink solids from the solutions. The precipitates were collected by vacuum filtration, washed several times with ethanol and allowed to air-dry. Deuterated samples were synthesised following a similar procedure but employing deuterated formic acid (formic acid-d<sub>2</sub>, 99+ atom % D, 95 % solution in D<sub>2</sub>O, Acros Organics) and deuterated ethanol (ethanol-d<sub>6</sub>, 99 atom % D, Acros Organics) as solvents instead. Phase purity was established using a Malvern Panalytical X'pert 3 powder diffractometer equipped with an Empyrean Cu LFF X-ray source (operated at 40 kV and 40 mA;  $\lambda_{\text{CuK}\alpha_1} = 1.5046 \text{ \AA}$ ,  $\lambda_{\text{CuK}\alpha_2} = 1.5444 \text{ \AA}$ ) and an X'Celerator line detector, with

ground samples mounted on zero-background silicon sample holders. Le Bail fits to the X-ray diffraction patterns were carried out using the programme Rietica [33,34], which were consistent with the formation of highly pure samples of the  $R3m \text{Ln}(\text{HCO}_2)_3$  phases (see Figs. S1 and S2 for quality of fits).

Compositional analysis of the  $\text{Ho}_{1-x}\text{Er}_x(\text{HCO}_2)_3$  series was carried out by energy dispersive X-Ray Fluorescence (EDXRF) measurements using a PANalytical Epsilon 3 spectrometer. The results were obtained by using a calibration curve determined from physically ground mixtures of  $\text{Ho}(\text{HCO}_2)_3$  and  $\text{Er}(\text{HCO}_2)_3$  with different Ho:Er molar ratios; namely, 92:8, 84:16, 75:25, 60:40, 40:60, 16:84 and 8:92. Scanning Electron Microscopy (SEM) measurements and further energy-dispersive X-ray spectroscopy analysis (EDX) on selected regions of the samples were carried out using a Hitachi S3400 N microscope to probe homogeneity. Powder samples were deposited on carbon tabs placed on aluminium sample holders without further preparation. Images of regions of approximately  $56 \times 44 \mu\text{m}^2$  were acquired using a 10 kV electron beam and a secondary electron (SE) detector.

Neutron diffraction patterns of  $\text{Ho}(\text{DCO}_2)_3$  were obtained using the WISH diffractometer at the ISIS Neutron and Muon Source [35]. Data from  $\text{Ho}(\text{DCO}_2)_3$  were obtained with the sample in a copper can cooled to low temperature using a  $^3\text{He}$  Heliox sorption refrigerator insert inside a standard Oxford Instruments cryostat. Measurements on  $\text{Er}(\text{DCO}_2)_3$  were performed using the Wombat diffractometer at the Australian Centre for Neutron Scattering, Australian Nuclear Science and Technology Organisation [36]. The  $\text{Er}(\text{DCO}_2)_3$  sample was placed in a copper can and cooled by a dilution fridge mounted inside a cryocooler with data collected using 2.41 Å neutrons. Diffraction patterns were fitted by the Rietveld method as implemented in FULLPROF with background fitted using a linear interpolation of points [37,38]. Peak shapes were fitted using a profile function built from a convolution of back-to-back exponentials with a pseudo-Voigt time-of-flight function for data collected by WISH or a pseudo-Voigt peak profile function with an axial divergence asymmetry correction for data collected by Wombat. Candidate magnetic structures were determined using ISODISTORT, which implements a distortion mode analysis approach [39]. Although both magnetic structures are in monoclinic space groups the lattice parameters were constrained to be orthogonal as the magneto-elastic coupling is small and did not cause any observable splitting in the diffraction pattern associated with  $\beta$  varying from 90°.

Magnetic property measurements were performed using a Quantum Design MPMS SQUID magnetometer, with a  $^3\text{He}$  insert utilised for measurements below 1.8 K. Samples were held in either a straw or a film with a uniform diamagnetic background. Heat capacity measurements were measured on a Quantum Design PPMS using a  $^3\text{He}$  insert to obtain data down to 400 mK; samples were ground into a fine powder and mixed with a silver addendum. The magnetic contribution to the heat capacity was then determined by subtracting the known silver contribution and lattice entropy, the latter using the Einstein-Debye equation [40].

## 3. Results and discussion

### 3.1. Physical property measurements of $\text{Ho}(\text{HCO}_2)_3$ and $\text{Er}(\text{HCO}_2)_3$

Since previous analysis of the diffuse magnetic scattering in  $\text{Ho}(\text{DCO}_2)_3$  suggested it has similar short range magnetic order as  $\text{Tb}(\text{DCO}_2)_3$  [27], physical property measurements were carried out to determine if TIA or the ECO phase emerged in  $\text{Ho}(\text{DCO}_2)_3$  below 1.5 K. Zero-field cooled magnetic susceptibility data for  $\text{Ho}(\text{HCO}_2)_3$  suggests a feature near 0.5 K (see Fig. 1a). While there is also a very small change in susceptibility at 1.5 K this coincides with where the MPMS switches between high and low temperature modes and is thought to be likely a result of this. A significant feature in the magnetic heat capacity of  $\text{Ho}(\text{HCO}_2)_3$  is observed near 1.2 K, suggesting a significant change in entropy at this point (see Fig. 1b). This peak broadens and moves to higher

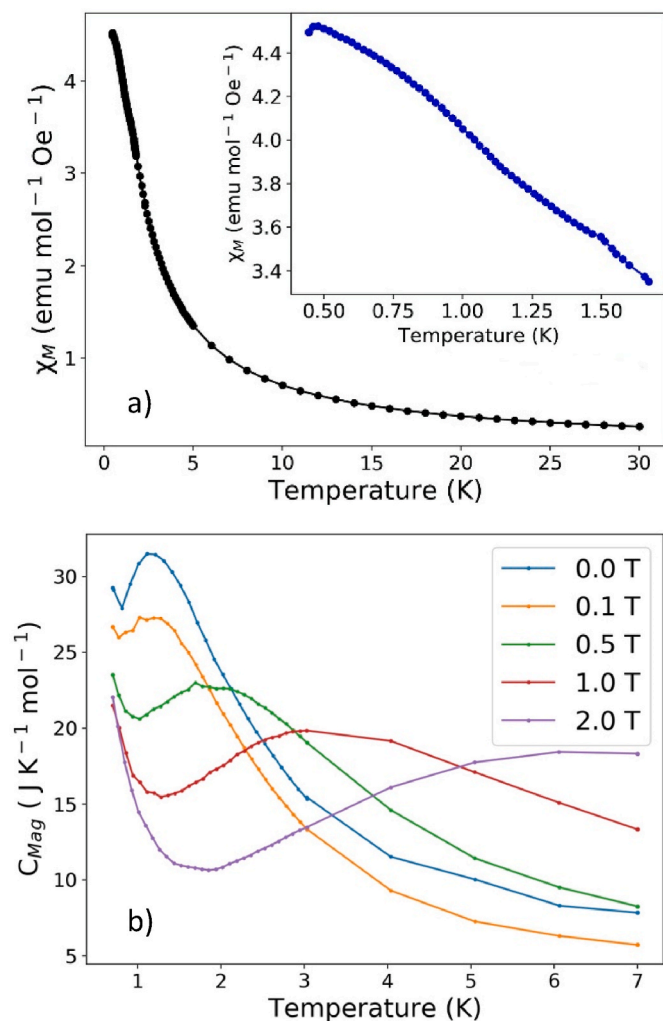


**Fig. 1.** a) Magnetic susceptibility of  $\text{Ho}(\text{HCO}_2)_3$  in a 100 Oe field below 30 K. The insert shows the low temperature region below 1.6 K. b) Magnetic heat capacity,  $C_{\text{Mag}}$ , of  $\text{Ho}(\text{HCO}_2)_3$  in variable fields between 400 mK and 14 K.

temperature under application of magnetic field, confirming it is magnetic in nature, with the broad nature of this feature suggestive of magnetic order with a finite correlation length. The heat capacity begins to increase again below 600 mK. Consistent with the limited field dependence of this feature this is expected to be caused by the hyperfine Schottky anomaly of Ho [41–43]. It does, however, overlap with the range in which a change is noted in the magnetic susceptibility suggesting a magnetic transition may also contribute to this.

Magnetic property measurements performed on  $\text{Er}(\text{DCO}_2)_3$  show no indication of long-range magnetic order forming down to 0.4 K (see Fig. 2a). Heat capacity data also show no significant features in the data, only increasing with lowering temperature, which can be ascribed to a Schottky anomaly (see Fig. 2b) [44].

Isothermal magnetization measurements of  $\text{Ho}(\text{HCO}_2)_3$  have been performed above and below the phase transitions. The results obtained are similar to those previously measured from  $\text{Ho}(\text{HCO}_2)_3$  at higher temperatures and saturating near  $g_J J/2$ , slightly above 2 T (see Fig. S3a). This is consistent with the behaviour expected for Ising spins, in agreement with the previous reverse Monte Carlo (RMC) fits to its magnetic diffuse scattering above 1.5 K [27]. Magnetization measurements of  $\text{Er}(\text{HCO}_2)_3$  also indicate an  $M_{\text{sat}}$  relatively close to  $g_J J/2$  suggesting that the spins also have significant single ion anisotropy (see Fig. S3b).

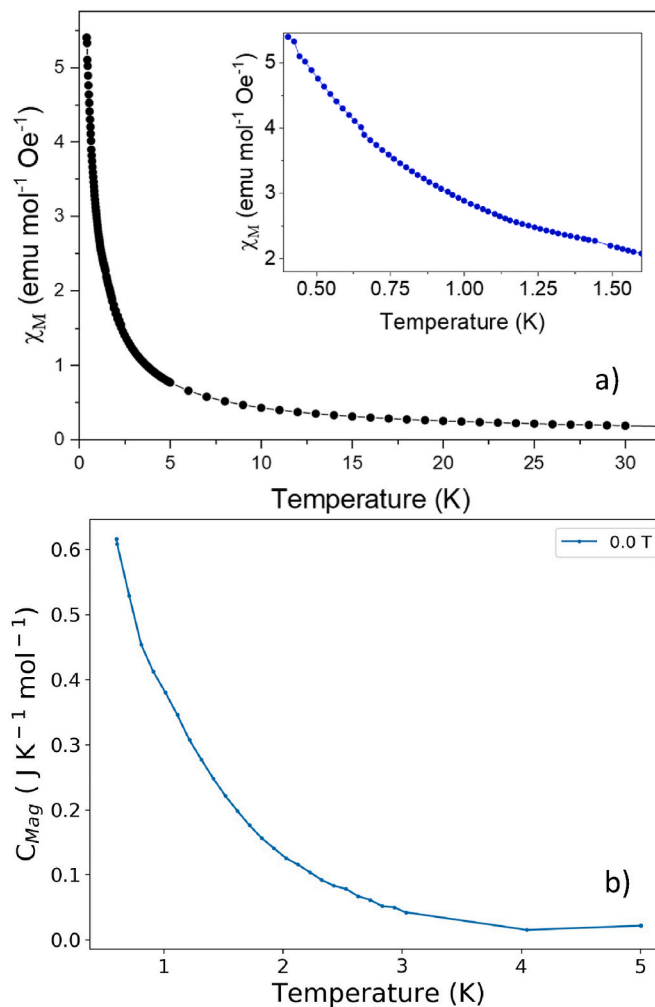


**Fig. 2.** a) Magnetic susceptibility of  $\text{Er}(\text{DCO}_2)_3$  in a 100 Oe field below 30 K. The insert shows the low temperature region below 1.6 K. b) Heat capacity measurements in zero applied field, of  $\text{Er}(\text{DCO}_2)_3$  between 0.5 and 5 K, indicating a lack of phase transitions.

### 3.2. Emergent charge order in $\text{Ho}(\text{HCO}_2)_3$

To facilitate the low temperature neutron diffraction study of  $\text{Ho}(\text{DCO}_2)_3$  it was cooled rapidly from 20 K to a base temperature of 0.25 K. Subsequent data collection reveals the presence of additional broad Bragg-like peaks in the neutron diffraction pattern, shown in Fig. 3. These did not change significantly in intensity or width when the sample was held at 0.25 K suggesting the magnetic phase did not evolve further with time at this temperature. These peaks closely resemble those from the ECO state of  $\text{Tb}(\text{DCO}_2)_3$  and were thus interpreted to be arising from a similar state [27]. The full-width half maximum (FWHM) of these magnetic peaks decreased with increasing temperature, indicating either the magnetic correlations or domains in  $\text{Ho}(\text{DCO}_2)_3$  were growing on heating, more likely this will be the later given magnetic correlations usually decrease with increasing temperature. It should be also pointed that local strains could be a contributing factor to the observed peak broadening in the rapidly cooled sample. This is unlikely in this case as the peaks arising from diffraction from the crystal structure do not show a similar broadening as those arising from magnetic reflection, as may be expected in cases where local strains in a system with magnetostriction are significant. These magnetic reflections are lost above 0.7 K, indicating the disappearance of this ordered magnetic phase. This is broadly consistent with the temperature at which the cusp in the magnetic susceptibility data occurs. It, however, varies significantly from the

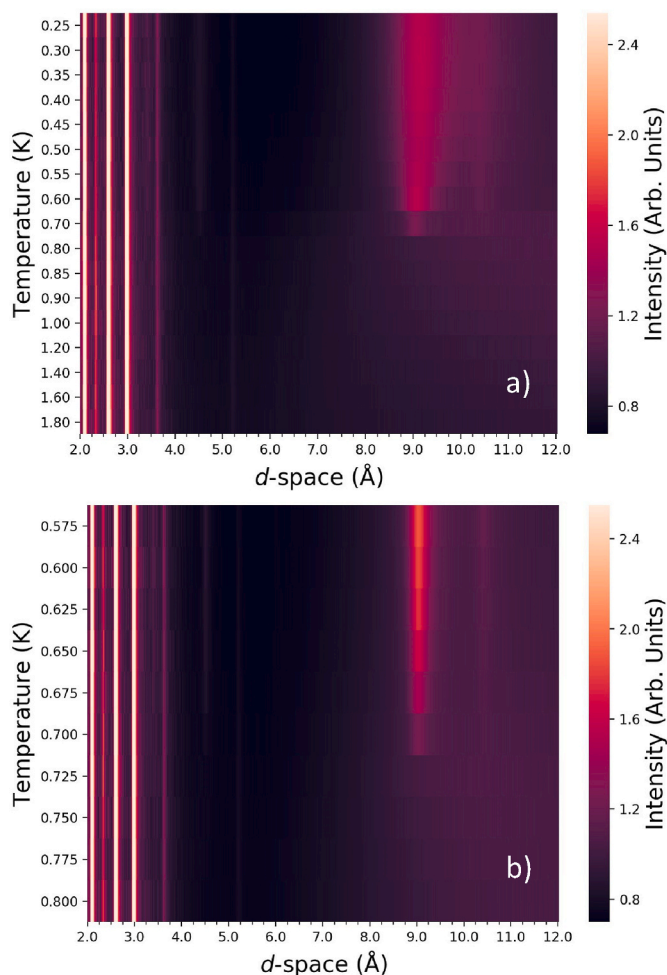


Fig. 3. Contour plots of neutron diffraction patterns of  $\text{Ho}(\text{DCO}_2)_3$  collected on a) warming and b) cooling.

feature observed in heat capacity measurements at 1.2 K; this may suggest there is some short-range order that significantly reduces the magnetic entropy of the system without leading to Bragg peaks in the neutron diffraction data. This would be consistent with the broad nature of the heat capacity signal and could be associated with the strong ferromagnetic correlations within the  $\text{HoO}_9$  chains previously reported near this temperature based on RMC fits to significant magnetic diffuse scattering [27]. We cannot, however, exclude the possibility of some sample dependence or discrepancy in actual sample temperature between the heat capacity measurements and results presented here.

To determine to what extent the broad magnetic peaks in  $\text{Ho}(\text{DCO}_2)_3$  arise from small magnetic domains caused by rapid cooling of the sample measurements were taken on cooling from 3 K to below  $T_N = 0.7$  K. Magnetic reflections appear at 0.7 K, indicating the transition temperature is not sensitive to whether it is approached by warming or cooling. The FWHM of peaks measured on gradual cooling were much sharper than those observed on rapid cooling through the magnetic phase transition, although they were still significantly broader than instrumental resolution. This indicates that the broadness of the magnetic peaks is intrinsic to the magnetic phase having a finite correlation length and not purely a result of finite magnetic domains emerging from the rapid cooling of the sample. It is likely that the greater peak broadening in the rapidly cooled sample compared to the more slowly cooled sample is caused by the magnetic domains being smaller in the former.

In  $\text{Tb}(\text{DCO}_2)_3$  the intermediate TIA state forms first, which is associated with a propagation vector  $\mathbf{k}_1$  of  $[0,0,1]$ , before additional

reflections appear at low temperature at a second propagation vector  $\mathbf{k}_2$  of  $[0,0.5,1]$ , indicating the emergence of the ECO state [27]. In  $\text{Ho}(\text{DCO}_2)_3$  all observed magnetic reflections appear simultaneously, suggesting its ECO state emerges immediately from the correlated paramagnetic phase. It was previously noted that, due to the appearance of the two  $\mathbf{k}$ -vectors at different temperatures in  $\text{Tb}(\text{DCO}_2)_3$ , the possibility of magnetic phase separation could not be ruled out [27]. That all magnetic reflections appear at the same temperature in  $\text{Ho}(\text{DCO}_2)_3$  suggests it is less likely phase segregation occurs, as is needed for the ECO state to be an accurate representation of the average magnetic phase of these materials.

As seen in  $\text{Tb}(\text{DCO}_2)_3$ , [27] the ordered magnetic phase of  $\text{Ho}(\text{DCO}_2)_3$  adopts the space group  $Pm'$  with magnetic moments along the chains, which run along the  $c$ -axis (see Fig. 4 for quality of fit and Table S1 for crystallographic parameters of nuclear phase). The bond valence method yielded a value of 3.04 for Ho, close to that expected for a  $\text{Ho}^{3+}$  ion [45]. The magnetic phase transition did not produce any significant change in the lattice parameters of  $\text{Ho}(\text{DCO}_2)_3$ , in either cooling or warming measurements. This suggests that such this deviation observed in  $\text{Tb}(\text{DCO}_2)_3$  is associated with the emergence of a TIA, which is absent in  $\text{Ho}(\text{DCO}_2)_3$ , and suggests the lack of significant magnetostriction in this material [27]. While in principle the reflections can be indexed with  $\mathbf{k}_2$  alone magnetic models using only this  $\mathbf{k}$ -vector did not match the intensities of the observed reflections well, including

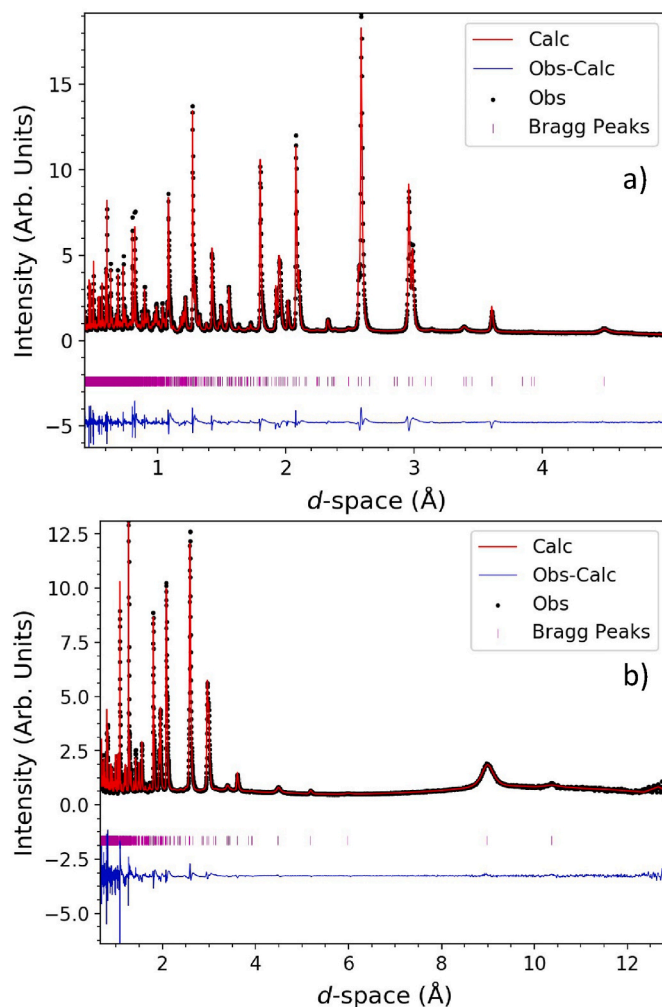
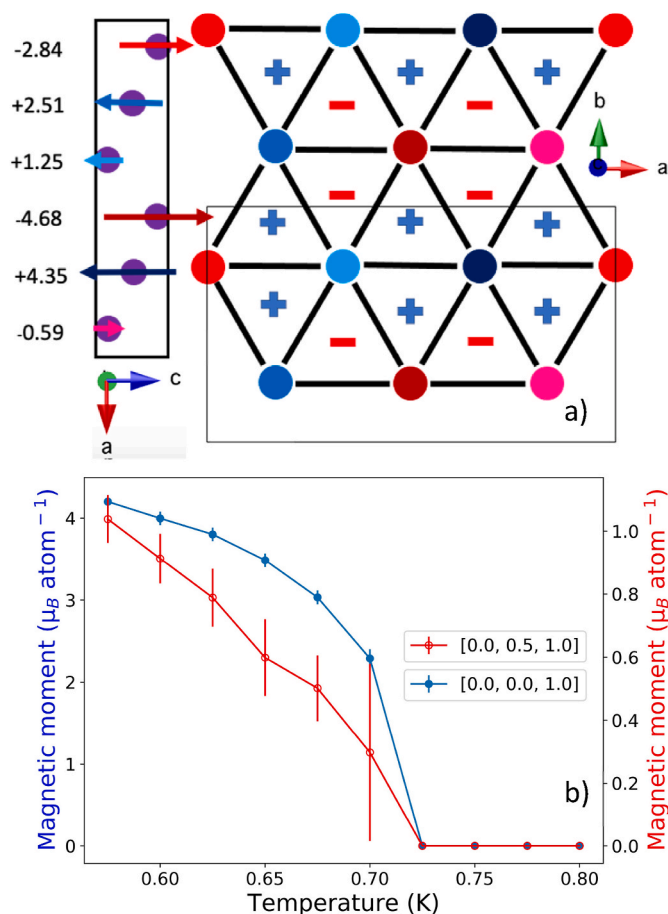


Fig. 4. Rietveld fits to neutron diffraction patterns of  $\text{Ho}(\text{DCO}_2)_3$  at 0.575 K from WISH along with the fitting statistics a) backscattering bank ( $2\theta$  of  $152.83^\circ$ ),  $R_p = 6.96\%$ ,  $R_{wp} = 7.08\%$  and b) bank 2/9 ( $2\theta$  of  $58.33^\circ$ ),  $R_p = 8.36\%$ ,  $R_{wp} = 4.87\%$ .

significantly underestimating the most intense reflection associated with the magnetic phase.

As previously discussed for  $\text{Tb}(\text{DCO}_2)_3$  the spin ordering derived from the propagation vector  $\mathbf{k}_1 = [0,0,1]$ , can be described by a spin density wave with moment along the  $c$ -axis [27]. Since with the resolution of our diffraction experiment the propagation vector seems to be locked to the commensurate vector (it is worth noting that (001) is not a special point of the Brillouin zone) different choices of the global magnetic phase will return equivalent fits to the data with a different arrangement of the spins on the triangles. When the phase is set to  $\pi/4$  the model resembles a partially disordered antiferromagnet (PDA) in which each of the triangles has one chain ordered with spin up, one down, and the third remaining disordered. The second phase choice,  $\pi/6$ , resembles an up-down-down model, which contains one chain moments ordered spin up and two chains with their moments-oriented spin down but with half the magnitude of the spin up chain. The  $\mathbf{k}_2$  propagation vector adds an extra modulation to the  $\mathbf{k}_1$  ordering between different chains. At a temperature of 0.575 K the sum of the spins on the chain around each triangle is  $\pm 0.92 \mu_B$  (see Fig. 5a) when the phase for the  $\mathbf{k}_1$  component is set to  $\pi/4$  and  $\pm 0.98 \mu_B$  when the phase is set to  $\pi/6$ . In this work we focus our analysis of the diffraction data assuming  $\pi/4$ , noting this does not alter the fundamental nature of the state observed but merely the value of the spins on each individual chain. Fig. 5b depicts the evolution of the Ho magnetic moment with respect to



**Fig. 5.** a)  $\text{Ho}(\text{DCO}_2)_3$  magnetic structure solution at 0.575 K where the global phase is set to  $\pi/4$ . Unit cell shown as black box with magnetic moments in  $Pm'$  space group with only Ho cation shown. The left-hand and right-hand sides of the panel shows projections in the  $ac$  plane and the  $ab$  plane, respectively. The spin charges are shown as minus and plus signs and circles and spins of the same colour correspond to Ho cations in chains with the same magnetic moment as each other. b) Evolution of the ordered magnetic moments associated with  $\mathbf{k}_1$  and  $\mathbf{k}_2$ , in  $\text{Ho}(\text{DCO}_2)_3$ , with respect to temperature.

temperature. The existence of the ECO phase in  $\text{Ho}(\text{DCO}_2)_3$ , as well as in  $\text{Tb}(\text{DCO}_2)_3$ , is likely a result of the similar combination of 1D ferromagnetic correlations and weaker antiferromagnetic interactions at higher temperatures between chains observed in previous Monte Carlo studies [24,27].

### 3.3. Antiferromagnetic chains in $\text{Er}(\text{DCO}_2)_3$

Upon cooling to 50 mK the neutron diffraction measurement performed on  $\text{Er}(\text{DCO}_2)_3$  show the appearance of extra weak reflections that can be attributed to the development of long-range magnetic ordering. These extra reflections can be indexed with the propagation vector  $\mathbf{k}_1 = [0, -0.5, 0.5]$ , corresponding to the  $L$ -point of the Brillouin zone. Given the moderate resolution of the Wombat diffractometer used for these measurements no conclusions can be drawn regarding the size of the magnetic correlations in  $\text{Er}(\text{DCO}_2)_3$ . The magnetic structure was refined against temperature subtracted data to best enable the weak magnetic reflections observed to be isolated. This involved subtracting the data collected at 6 K from that obtained at 50 mK after first refining the crystal structure against data at 50 mK (see Table S2 for crystallographic parameters and Fig. S4 for the quality of the fit). The calculation of bond valence sums resulted in a value of 2.98 for Er, close to that expected for a  $\text{Er}^{3+}$  ion [45]. The best fits for the reflections observed is obtained with an antiferromagnetic structure in space group  $C_{2c}$  (see Fig. 6 for the quality of the fit and Fig. 7 for a depiction of this magnetic phase). In this structure there is only one independent Er site with an ordered magnetic moment of  $0.75(4) \mu_B$  at base temperature, lying in the  $ab$  plane oriented along the  $[0.72, -0.22, 0]$  vector. The low magnetic moment obtained suggests the material may only be slightly below its ordering temperature, which is confirmed by the magnetic reflections being lost on heating between 50 and 100 mK.  $\text{Er}(\text{DCO}_2)_3$  has antiferromagnetic order within its chains, unlike the ferromagnetic coupling in  $\text{Tb}(\text{DCO}_2)_3$  and  $\text{Ho}(\text{DCO}_2)_3$ . Indeed such interactions within the chains is directly implied by the magnetic  $\mathbf{k}$ -vector of  $\text{Er}(\text{DCO}_2)_3$ .

### 3.4. Magnetic properties of the $\text{Ho}_{1-x}\text{Er}_x(\text{HCO}_2)_3$ series

That  $\text{Er}(\text{DCO}_2)_3$  has antiferromagnetic coupling within its chains, in contrast to the ferromagnetic chains in  $\text{Tb}(\text{DCO}_2)_3$  and  $\text{Ho}(\text{DCO}_2)_3$  is an interesting observation [27]. It offers the potential to create a series of materials with a mixture of ferromagnetic and antiferromagnetic intra-chain coupling. In the ideal case this would lead to a random spin chain paramagnet in which there is a random distribution of ferromagnetic

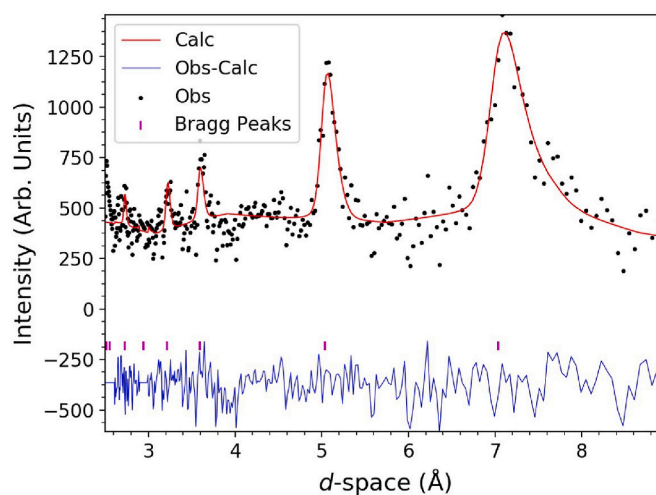


**Fig. 6.** Temperature subtracted “magnetic only” neutron diffraction pattern fit of  $\text{Er}(\text{DCO}_2)_3$  at 50 mK, using a  $2.41 \text{ \AA}$  wavelength. The fit to the data yielded the fitting statistics, for the magnetic phase, of  $R_p = 13.5 \%$ , and  $R_{wp} = 15.8 \%$ .

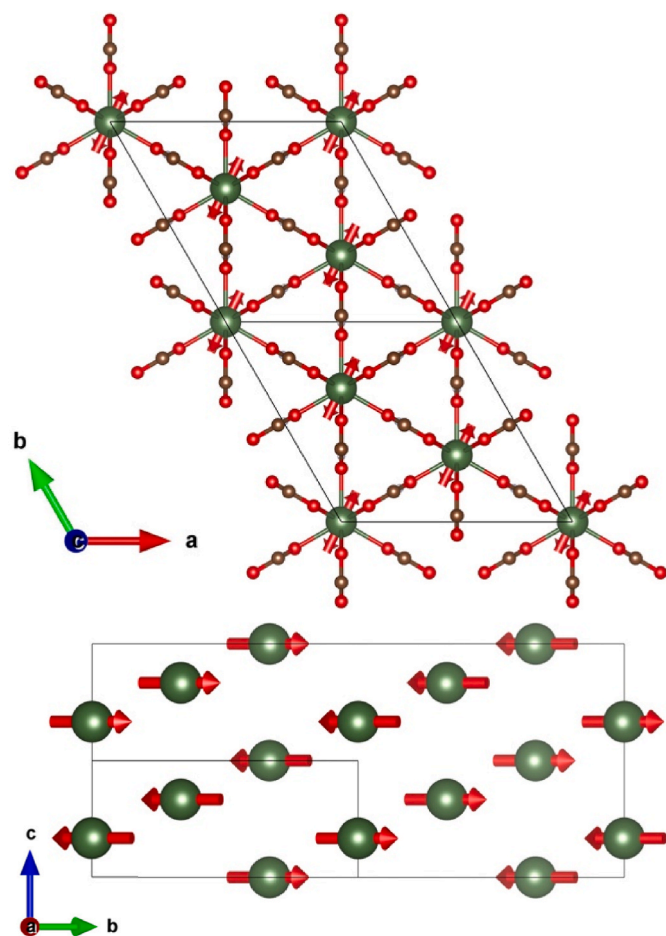


**Fig. 7.** Antiferromagnetic structure of  $\text{Er}(\text{DCO}_2)_3$  at 50 mK. Erbium, oxygen, hydrogen and carbon atoms are shown as green, red, grey and black sphere; the view of the  $bc$  plane shows only the erbium atoms for clarity. Unit cell shown in black.

and antiferromagnetic intrachain coupling [11]. Since the lower magnetic ordering temperature suggests the magnetic coupling in  $\text{Er}(\text{HCO}_2)_3$  may be relatively weak a solid solution with  $\text{Ho}(\text{HCO}_2)_3$  to make the  $\text{Ho}_{1-x}\text{Er}_x(\text{HCO}_2)_3$  series is likely a suitable way of studying this since it is known the magnetic correlations within  $\text{Ho}(\text{DCO}_2)_3$  are weaker than  $\text{Tb}(\text{DCO}_2)_3$  [24,27].

XRF measurements indicated that samples of  $\text{Ho}_{1-x}\text{Er}_x(\text{HCO}_2)_3$  had stoichiometries close to the nominal composition (see Table S3). The value of  $x$  determined from these measurements is consistently 0.03–0.04 mol less than expected, this may indicate that Ho is preferentially being incorporated or that there is a small systematic error with in calibrated values determined from XRF measurements. Additional composition analysis carried out via EDX on selected regions of samples (see Figs. S5–S13 and Tables S4–S12) showed good agreement with values determined from bulk XRF experiments with no obvious indication of sample inhomogeneity. Consistent with this lattice parameters obtained from Le Bail refinements gradually decreased with increasing  $x$  (see Fig. S14 and Table S13), although this trend is not linear. This is likely due to the very small change in the ionic radii of  $\text{Ho}^{3+}$  and  $\text{Er}^{3+}$  (*c.f.* 1.072 and 1.062 Å for 9-coordinate  $\text{Ho}^{3+}$  and  $\text{Er}^{3+}$ , respectively) [46] amplifying small inaccuracies in the determination of the lattice parameters.

Bulk magnetic measurements were carried out for  $\text{Ho}_{1-x}\text{Er}_x(\text{HCO}_2)_3$ , with  $x = 0.20, 0.40, 0.60$  and  $0.80$  (see Fig. S15) between 1.8 and 300 K with more extensive measurements of the  $x = 0.50$  measured down to 400 mK (see Fig. 8). All the sample measured show paramagnetic

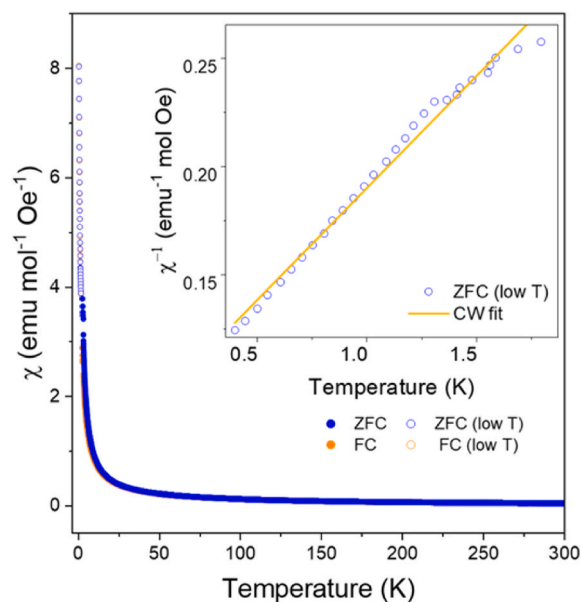


**Fig. 8.** Bulk magnetic properties of  $\text{Ho}_{0.5}\text{Er}_{0.5}(\text{HCO}_2)_3$  measured between 0.4 and 1.8 K (hollow symbols) and from 1.8 to 300 K (full symbols) using a 1000 Oe applied field. The inset shows the Curie-Weiss fit to the inverse magnetic susceptibility  $\chi^{-1}$  across the lower temperature range.

behaviour down to 1.8 K, similar to that of the parent compounds. Linear behaviour of the inverse susceptibility  $\chi^{-1}(T)$ , consistent with the Curie-Weiss law, can be observed across the  $\text{Ho}_{1-x}\text{Er}_x(\text{HCO}_2)_3$  series down to  $\sim 30$  K, with deviation from linearity below this temperature that are likely due to crystal field effects. Fits to the inverse susceptibility  $\chi^{-1}(T)$  using the Curie-Weiss law were therefore carried out from 30 to 300 K and 2 to  $\sim 15$  or  $\sim 20$  K, for lower temperatures, with the exception of  $\text{Ho}_{0.5}\text{Er}_{0.5}(\text{HCO}_2)_3$ , for which low-temperature fits were carried out from 0.4 to 1.5 K (see Figs. S15–S19 with statistical measures of the qualities of these fits presented in Table S14), with results reported in Table 1. The Weiss constants extracted from the low temperature fits should be less affected by crystal field effects and, thus, give the best insight into the low temperature interactions in these mixed phases. The values obtained are consistent with weak antiferromagnetic interactions across the series, although this value increases with Er concentration as would be expected from the switch from ferromagnetic intrachain coupling in  $\text{Ho}(\text{HCO}_2)_3$  to antiferromagnetic coupling in  $\text{Er}(\text{HCO}_2)_3$ . Examining the effective magnetic moment extracted from the fit to the high temperature region, since crystal field effects partially quench the orbital angular moment at lower temperatures, it can be seen that the moment

**Table 1**

Curie-Weiss temperature  $\theta_{\text{CW}}$  and effective magnetic moments  $\mu_{\text{eff}}$  from the Curie-Weiss fit of the inverse susceptibility  $\chi^{-1}(T)$  of  $\text{Ho}_{1-x}\text{Er}_x(\text{HCO}_2)_3$  series.

$x$	Range (K)	$\theta_{\text{CW}}$ (K)	$\mu_{\text{eff}}$ ( $\mu_{\text{B}}$ )	Range (K)	$\theta_{\text{CW}}$ (K)	$\mu_{\text{eff}}$ ( $\mu_{\text{B}}$ )
0	30–300	−10.95 (15)	10.545(4)	2–15	−0.54 (4)	9.127 (12)
0.20	30–300	−11.60 (5)	10.850(2)	2–15	−0.62 (4)	7.61(4)
0.40	30–300	−12.21 (4)	10.9145 (14)	2–15	−0.96 (6)	8.59(2)
0.50	30–300	−11.00 (2)	10.4154 (8)	0.4–1.5	−0.72 (2)	8.47(5)
0.60	30–300	−13.38 (4)	10.6284 (10)	2–20	−0.99 (6)	9.18(2)
0.80	30–300	−15.98 (13)	9.74(4)	2–20	−1.22 (10)	9.243 (15)
1.00	30–300	−16.13 (8)	9.68(2)	2–20	−2.20 (2)	7.64(5)

generally decreases with Er doping, consistent with  $\text{Er}^{3+}$  being expected to have a smaller moment than  $\text{Ho}^{3+}$  according to the Russell-Saunders coupling scheme. The change in effective moment with  $x$  is, however, not smooth with a particularly notable increase between the  $x = 0$  and 0.20 samples and a significant decrease between the  $x = 0.60$  and 0.80 samples. While some of these deviations from the expected trend may arise from experimental error it is likely that subtle distortions to the local coordination environment with  $x$  leads to a change in the crystal field that affects the contribution from the orbital angular momentum for a particular cation. In particular for values of  $x \sim 0.2$  the contribution from the orbital angular momentum increases more than expected and then between 0.60 and 0.80 there is a significant decrease in the contribution from the orbital angular momentum [47].

Notably,  $\text{Ho}_{1-x}\text{Er}_x(\text{HCO}_2)_3$  maintains a linear trend in its inverse susceptibility across the low temperature regime down to 0.4 K. This is promising with respect to the potential of this compound to host a random spin chain paramagnet containing an equal mixture of antiferromagnetic and ferromagnetic coupling randomly distributed throughout its chains [11]. More detailed analysis of  $\text{Ho}_{0.5}\text{Er}_{0.5}(\text{HCO}_2)_3$  is required to establish if such a state is present in this material, likely using elastic and inelastic neutron scattering to study it on the atomic level. We would note that this material, is however, the first potential candidate to host such a state that is accessible using neutron scattering since studies of the local magnetic correlations of the only other candidate phases,  $\text{Sr}_3\text{CuPt}_{1-x}\text{Ir}_x\text{O}_6$ , are restricted by the presence of highly neutron absorbing Ir in light of the  $s = \frac{1}{2}$  magnetic moments in the compound [11].

#### 4. Conclusions

In this work we have probed the magnetic ordering of  $\text{Ho}(\text{HCO}_2)_3$  and  $\text{Er}(\text{HCO}_2)_3$ .  $\text{Ho}(\text{HCO}_2)_3$  has been found to adopt a similar magnetic ECO phase to the low temperature phase in  $\text{Tb}(\text{HCO}_2)_3$  below 1.2 K. In this phase, which has magnetic moments along the chain direction, the magnetic moment of the cations in neighbouring chains vary but the total around a triangle remains the same, which can be interpreted as an emergent magnetic change.  $\text{Ho}(\text{HCO}_2)_3$ , however, lacks the intermediate TIA phase found in  $\text{Tb}(\text{HCO}_2)_3$  with the emergence of all magnetic reflections at the same temperature, which makes magnetic phase segregation in  $\text{Ho}(\text{HCO}_2)_3$  unlikely. There also appears to be a clear cooling rate dependence on the size of the magnetic domains in  $\text{Ho}(\text{HCO}_2)_3$ . In contrast to the ferromagnetic correlations within the chains of  $\text{Tb}(\text{HCO}_2)_3$  and  $\text{Ho}(\text{HCO}_2)_3$  Er adopts an ordered state with antiferromagnetic coupling within its chains, with the spins lying in the  $ab$  plane. A series of  $\text{Ho}_{1-x}\text{Er}_x(\text{HCO}_2)_3$  was made to explore the possibility of making compounds with a mixture of ferromagnetic and antiferromagnetic coupling within the chains. It was found that the  $\text{Ho}_{0.5}\text{Er}_{0.5}(\text{HCO}_2)_3$  member of this series remained paramagnetic down to 0.4 K, making it a potential starting point to search for a random spin chain paramagnet.

#### CRedit authorship contribution statement

**Richard J.C. Dixey:** Writing – review & editing, Visualization, Validation, Investigation, Formal analysis. **Mario Falsaperna:** Writing – review & editing, Visualization, Validation, Investigation, Formal analysis. **Jonathan M. Bulled:** Writing – review & editing, Investigation. **Fabio Orlandi:** Writing – review & editing, Investigation. **Pascal Manuel:** Writing – review & editing, Investigation. **James R. Hester:** Writing – review & editing, Investigation. **Paromita Mukherjee:** Writing – review & editing, Investigation. **Sián E. Dutton:** Writing – review & editing, Investigation. **Paul J. Saines:** Writing – review & editing, Writing – original draft, Supervision, Funding acquisition, Conceptualization.

#### Declaration of competing interest

The authors declare that they have no known competing financial interests or personal relationships that could have appeared to influence the work reported in this paper.

#### Data availability

Data will be made available on request.

#### Acknowledgements

We would like to thank the Leverhulme Trust for funding via RPG-2018-268. R.J.C.D. would like to acknowledge the University of Kent for financial support through the provision of a Vice-Chancellors scholarship and P.J.S. would like to thank the Royal Society of Chemistry for support through a researcher mobility grant. The authors would like to thank the Science and Technologies Facilities Council for access to the ISIS facility at Harwell (data set <https://doi.org/10.5286/ISIS.E.99687059>) and the Australian Government for access to the Australian Centre for Neutron Scattering (proposal 6430). Low temperature MPMS measurements were carried out on the EPSRC Advanced Materials Characterisation Suite (EP1M0052411).

#### Appendix A. Supplementary data

Supplementary data to this article can be found online at <https://doi.org/10.1016/j.jssc.2024.124770>.

#### References

- [1] M. Steiner, J. Villain, C.G. Windsor, Theoretical and experimental studies on one-dimensional magnetic systems, *Adv. Phys.* 25 (1976) 87–209, <https://doi.org/10.1080/00018737600101372>.
- [2] H.-J. Mikeska, M. Steiner, Solitary excitations in one-dimensional magnets, *Adv. Phys.* 40 (1991) 191–356, <https://doi.org/10.1080/00018739100101492>.
- [3] J.K. Kjems, M. Steiner, Evidence for soliton modes in the one-dimensional ferromagnet  $\text{CsNiF}_3$ , *Phys. Rev. Lett.* 41 (1978) 1137–1140, <https://doi.org/10.1103/PhysRevLett.41.1137>.
- [4] A.P. Ramirez, W.P. Wolf, Specific heat of  $\text{CsNiF}_3$ : evidence for spin solitons, *Phys. Rev. Lett.* 49 (1982) 227–230, <https://doi.org/10.1103/PhysRevLett.49.227>.
- [5] H.P. Bader, R. Schilling, Conditions for a ferromagnetic ground state of Heisenberg Hamiltonians, *Phys. Rev. B* 19 (1979) 3556–3560, <https://doi.org/10.1103/PhysRevB.19.3556>.
- [6] T. Hamada, J. Kane, S. Nakagawa, Y. Natsume, Exact solution of ground state for uniformly distributed RVB in one-dimensional spin-1/2 heisenberg systems with frustration, *J. Phys. Soc. Japan* 57 (1988) 1891–1894, <https://doi.org/10.1143/JPSJ.57.1891>.
- [7] M. Hase, I. Terasaki, K. Uchinokura, Observation of the spin-Peierls transition in linear  $\text{Cu}^{2+}$  (spin-1/2) chains in an inorganic compound  $\text{CuGeO}_3$ , *Phys. Rev. Lett.* 70 (1993) 3651–3654, <https://doi.org/10.1103/PhysRevLett.70.3651>.
- [8] Q.J. Harris, Q. Feng, R.J. Birgeneau, K. Hirota, K. Kakurai, J.E. Lorenzo, G. Shirane, M. Hase, K. Uchinokura, H. Kojima, I. Tanaka, Y. Shibuya, Thermal contraction at the spin-Peierls transition in  $\text{CuGeO}_3$ , *Phys. Rev. B* 50 (1994) 12606–12610, <https://doi.org/10.1103/PhysRevB.50.12606>.
- [9] M. Boehm, S. Coad, B. Roessli, A. Zheludev, M. Zolliker, P. Böni, D. McK. Paul, H. Eisaki, N. Motoyama, S. Uchida, Competing exchange interactions in  $\text{Li}_2\text{CuO}_2$ , *Europhys. Lett.* 43 (1998) 77, <https://doi.org/10.1209/epl/i1998-00322-3>.
- [10] S.E. Dutton, M. Kumar, M. Mourigal, Z.G. Soos, J.-J. Wen, C.L. Broholm, N. H. Andersen, Q. Huang, M. Zbiri, R. Toft-Petersen, R.J. Cava, Quantum spin liquid in frustrated one-dimensional  $\text{LiCuSbO}_4$ , *Phys. Rev. Lett.* 108 (2012) 187206, <https://doi.org/10.1103/PhysRevLett.108.187206>.
- [11] T.N. Nguyen, P.A. Lee, H.-C. zur Loye, Design of a random quantum spin chain paramagnet:  $\text{Sr}_3\text{CuPt}_{0.5}\text{Ir}_{0.5}\text{O}_6$ , *Science* 271 (1996) 489–491, <https://doi.org/10.1126/science.271.5248.489>.
- [12] S.H. Irons, T.D. Sangrey, K.M. Beauchamp, M.D. Smith, H.-C. zur Loye, Ac susceptibility of  $\text{Sr}_3\text{CuPt}_{1-x}\text{Ir}_x\text{O}_6$ : a magnetic system with competing interactions and dimensionality, *Phys. Rev. B* 61 (2000) 11594–11600, <https://doi.org/10.1103/PhysRevB.61.11594>.
- [13] A. Niazi, E.V. Sampathkumaran, P.L. Paulose, D. Eckert, A. Handstein, K.-H. Müller,  $\text{Sr}_3\text{CuIrO}_6$ , a spin-chain compound with random ferromagnetic–antiferromagnetic interactions, *Solid State Commun.* 120 (2001) 11–15, [https://doi.org/10.1016/S0038-1098\(01\)00313-1](https://doi.org/10.1016/S0038-1098(01)00313-1).
- [14] S. Sahling, G. Remenyi, C. Paulsen, P. Monceau, V. Saligram, C. Marin, A. Revcolevschi, L.P. Regnault, S. Raymond, J.E. Lorenzo, Experimental realization of long-distance entanglement between spins in antiferromagnetic quantum spin chains, *Nat. Phys.* 11 (2015) 255–260, <https://doi.org/10.1038/nphys3186>.

- [15] P.J. Saines, N.C. Bristowe, Probing magnetic interactions in metal–organic frameworks and coordination polymers microscopically, *Dalt. Trans.* 47 (2018) 13257–13280, <https://doi.org/10.1039/C8DT02411A>.
- [16] A.E. Thorarindottir, T.D. Harris, Metal–organic framework magnets, *Chem. Rev.* 120 (2020) 8716–8789, <https://doi.org/10.1021/acs.chemrev.9b00666>.
- [17] G. Mínguez Espallargas, E. Coronado, Magnetic functionalities in MOFs: from the framework to the pore, *Chem. Soc. Rev.* 47 (2018) 533–557, <https://doi.org/10.1039/C7CS00653E>.
- [18] A.K. Cheetham, C.N.R. Rao, R.K. Feller, Structural diversity and chemical trends in hybrid inorganic–organic framework materials, *Chem. Commun.* (2006) 4780–4795, <https://doi.org/10.1039/B610264F>.
- [19] Z. Duan, Z. Wang, S. Gao, Irreversible transformation of chiral to achiral polymorph of  $K[Co(HCOO)_3]$ : synthesis, structures, and magnetic properties, *Dalt. Trans.* 40 (2011) 4465–4473, <https://doi.org/10.1039/C0DT01701A>.
- [20] M.B. Hursthouse, M.E. Light, D.J. Price, One-dimensional magnetism in anhydrous iron and cobalt ternary oxalates with rare trigonal-prismatic metal coordination environment, *Angew. Chem. Int. Ed.* 43 (2004) 472–475, <https://doi.org/10.1002/anie.200352406>.
- [21] P.J. Saines, M. Steinmann, J.-C. Tan, H.H.-M. Yeung, W. Li, P.T. Barton, A. K. Cheetham, Isomer-directed structural diversity and its effect on the nanosheet exfoliation and magnetic properties of 2,3-dimethylsuccinate hybrid frameworks, *Inorg. Chem.* 51 (2012) 11198–11209, <https://doi.org/10.1021/ic302011x>.
- [22] P.J. Saines, J.-C. Tan, H.H.-M. Yeung, P.T. Barton, A.K. Cheetham, Layered inorganic–organic frameworks based on the 2,2-dimethylsuccinate ligand: structural diversity and its effect on nanosheet exfoliation and magnetic properties, *Dalt. Trans.* 41 (2012) 8585–8593, <https://doi.org/10.1039/C2DT30648D>.
- [23] G. Lorusso, J.W. Sharples, E. Palacios, O. Roubeau, E.K. Brechin, R. Sessoli, A. Rossin, F. Tuna, E.J.L. McInnes, D. Collison, M. Evangelisti, A dense metal–organic framework for enhanced magnetic refrigeration, *Adv. Mater.* 25 (2013) 4653–4656, <https://doi.org/10.1002/adma.201301997>.
- [24] P.J. Saines, J.A.M. Paddison, P.M.M. Thygesen, M.G. Tucker, Searching beyond Gd for magnetocaloric frameworks: magnetic properties and interactions of the Ln  $(HCO_2)_3$  series, *Mater. Horiz.* 2 (2015) 528–535, <https://doi.org/10.1039/C5MH000113G>.
- [25] R.J.C. Dixey, P. Manuel, F. Orlandi, P. Mukherjee, S.E. Dutton, G.B.G. Stenning, P. J. Saines, In situ observation of the magnetocaloric effect through neutron diffraction in the  $Tb(DCO_2)_3$  and  $TbODCO_3$  frameworks, *J. Mater. Chem. C* 8 (2020) 12123–12132, <https://doi.org/10.1039/d0tc03153d>.
- [26] D.R. Harcombe, P.G. Welch, P. Manuel, P.J. Saines, A.L. Goodwin, One-dimensional magnetic order in the metal-organic framework  $Tb(HCO_2)_3$ , *Phys. Rev. B* 94 (2016) 174429, <https://doi.org/10.1103/PhysRevB.94.174429>.
- [27] R.J.C. Dixey, F. Orlandi, P. Manuel, P. Mukherjee, S.E. Dutton, P.J. Saines, Emergent magnetic order and correlated disorder in formate metal-organic frameworks, *Philos. Trans. R. Soc. A Math. Phys. Eng. Sci.* 377 (2019) 20190007, <https://doi.org/10.1098/rsta.2019.0007>.
- [28] K. Matsuhira, Z. Hiroi, T. Tayama, S. Takagi, T. Sakakibara, A new macroscopically degenerate ground state in the spin ice compound  $Dy_2Ti_2O_7$  under a magnetic field, *J. Phys. Condens. Matter* 14 (2002) L559, <https://doi.org/10.1088/0953-8984/14/29/101>.
- [29] T. Fennell, S.T. Bramwell, D.F. McMorrow, P. Manuel, A.R. Wildes, Pinch points and Kasteleyn transitions in Kagome ice, *Nat. Phys.* 3 (2007) 566–572, <https://doi.org/10.1038/nphys632>.
- [30] J.A.M. Paddison, H.S. Ong, J.O. Hamp, P. Mukherjee, X. Bai, M.G. Tucker, N. P. Butch, C. Castelnovo, M. Mourigal, S.E. Dutton, Emergent order in the Kagome Ising magnet  $Dy_3Mg_2Sb_3O_{14}$ , *Nat. Commun.* 7 (2016) 13842, <https://doi.org/10.1038/ncomms13842>.
- [31] R. Dixey, Ferromagnetic Ising Chains in Frustrated Magnetocaloric Frameworks, University of Kent, 2020. <https://kar.kent.ac.uk/80771/>.
- [32] M. Falsaperna, Influence of Structure and Doping on Frustration in Low-Dimensional Coordination Polymers, University of Kent, 2022, <https://doi.org/10.22024/UniKent/01.02.97317>.
- [33] A. Le Bail, H. Duroy, J.L. Fourquet, Ab-initio structure determination of  $LiSbWO_6$  by X-ray powder diffraction, *Mater. Res. Bull.* 23 (1988) 447–452, [https://doi.org/10.1016/0025-5408\(88\)90019-0](https://doi.org/10.1016/0025-5408(88)90019-0).
- [34] B.A. Hunter, C.J. Howard, A Computer Program for Rietveld Analysis of X-Ray and Neutron Powder Diffraction Patterns, 1998.
- [35] L.C. Chapon, P. Manuel, P.G. Radaelli, C. Benson, L. Perrott, S. Ansell, N.J. Rhodes, D. Raspino, D. Duxbury, E. Spill, J. Norris, Wish: the New Powder and Single Crystal Magnetic Diffractometer on the Second Target Station, *Neutron News*, vol. 22, 2011, pp. 22–25, <https://doi.org/10.1080/10448632.2011.569650>.
- [36] A.J. Studer, M.E. Hagen, T.J. Noakes, Wombat: the high-intensity powder diffractometer at the OPAL reactor, *Phys. B Condens. Matter* 385–386 (2006) 1013–1015, <https://doi.org/10.1016/j.physb.2006.05.323>.
- [37] H.M. Rietveld, A profile refinement method for nuclear and magnetic structures, *J. Appl. Crystallogr.* 2 (1969) 65–71, <https://doi.org/10.1107/S0021889869006558>.
- [38] J. Rodríguez-Carvajal, Recent advances in magnetic structure determination by neutron powder diffraction, *Phys. B Phys. Condens. Matter.* 192 (1993) 55–69, [https://doi.org/10.1016/0921-4526\(93\)90108-1](https://doi.org/10.1016/0921-4526(93)90108-1).
- [39] B.J. Campbell, H.T. Stokes, D.E. Tanner, D.M. Hatch, ISODISPLACE: a web-based tool for exploring structural distortions, *J. Appl. Crystallogr.* 39 (2006) 607–614, <https://doi.org/10.1107/S0021889806014075>.
- [40] D.R. Smith, F.R. Fickett, Low-temperature properties of silver, *J. Res. Natl. Inst. Stand. Technol.* 100 (1995) 119–171, <https://doi.org/10.6028/jres.100.012>.
- [41] E.C. Heltemes, C.A. Swenson, Nuclear contribution to the heat capacity of terbium metal, *J. Chem. Phys.* 35 (2004) 1264–1265, <https://doi.org/10.1063/1.1732033>.
- [42] D. Neogy, P. Paul, K.N. Chattopadhyay, Investigation of magnetic, thermal and hyperfine properties of  $Tb^{3+}$  in the single crystal of terbium trifluoromethanesulfonate nonahydrate, *J. Magn. Magn. Mater.* 283 (2004) 164–170, <https://doi.org/10.1016/j.jmmm.2004.05.018>.
- [43] J. Hamman, P. Manneville, Ordre magnétique électronique induit par les interactions hyperfines dans les grenats de gallium-holmium et de gallium-terbium, *J. Phys. Fr.* 34 (1973) 615–622, <https://doi.org/10.1051/jphys:01973003407061500>.
- [44] A. Tari, *The Specific Heat of Matter at Low Temperatures*, World Scientific, 2003.
- [45] I.D. Brown, D. Altermatt, Bond-valence parameters obtained from a systematic analysis of the inorganic crystal structure database, *Acta Crystallogr. B* 41 (1985) 244–247, <https://doi.org/10.1107/S0108768185002063>.
- [46] R.D. Shannon, Revised effective ionic radii and systematic studies of interatomic distances in halides and chalcogenides, *Acta Crystallogr., Sect. A* 32 (1976) 751–767, <https://doi.org/10.1107/S0567739476001551>.
- [47] J.L. Manson, S.P.M. Curley, R.C. Williams, D. Walker, P.A. Goddard, A. Ozarowski, R.D. Johnson, A.M. Vibhakar, D.Y. Villa, M.L. Rhodehouse, S.M. Birnbaum, J. Singleton, Controlling magnetic anisotropy in a zero-dimensional  $S = 1$  magnet using isotropic cation substitution, *J. Am. Chem. Soc.* 143 (2021) 4633–4638, <https://doi.org/10.1021/jacs.0c12516>.